Global and Planetary Change 68 (2009) 209–224

Contents lists available at ScienceDirect

Global and Planetary Change

journal homepage: www.elsevier.com/locate/gloplacha

Climatic changes and associated impacts in the Mediterranean resulting from a 2 °C global warming

C. Giannakopoulos [a,*], P. Le Sager [a,b], M. Bindi [c], M. Moriondo [d], E. Kostopoulou [a], C.M. Goodess [e]

[a] Institute for Environmental Research and Sustainable Development, National Observatory of Athens, I. Metaxa and V. Pavlou, GR15236 Palaia Pendeli, Athens, Greece
[b] Atmospheric Chemistry Modelling, Division of Engineering and Applied Science, Harvard University, Cambridge, MA 02138, USA
[c] Department of Agronomy and Land Management, University of Florence, 50144 Florence, Italy
[d] CNR-IBIMET, Via G. Caproni 8, 50145 Florence, Italy
[e] Climatic Research Unit, University of East Anglia, Norwich, NR4 7TJ, United Kingdom

ARTICLE INFO

Article history:
Received 16 October 2008
Accepted 2 June 2009
Available online 10 June 2009

Keywords:
Mediterranean
climate change
extremes
bootstrap
impacts
energy
agriculture
forest fires

ABSTRACT

Climatic changes over the Mediterranean basin in 2031–2060, when a 2 °C global warming is most likely to occur, are investigated with the HadCM3 global circulation model and their impacts on human activities and natural ecosystem are assessed. Precipitation and surface temperature changes are examined through mean and extreme values analysis, under the A2 and B2 emission scenarios. Confidence in results is obtained via bootstrapping. Over the land areas, the warming is larger than the global average. The rate of warming is found to be around 2 °C in spring and winter, while it reaches 4 °C in summer. An additional month of summer days is expected, along with 2–4 weeks of tropical nights. Increase in heatwave days and decrease in frost nights are expected to be a month inland. In the northern part of the basin the widespread drop in summer rainfall is partially compensated by a winter precipitation increase. One to 3 weeks of additional dry days lead to a dry season lengthened by a week and shifted toward spring in the south of France and inland Algeria, and autumn elsewhere. In central Mediterranean droughts are extended by a month, starting a week earlier and ending 3 weeks later. The impacts of these climatic changes on human activities such as agriculture, energy, tourism and natural ecosystems (forest fires) are also assessed. Regarding agriculture, crops whose growing cycle occurs mostly in autumn and winter show no changes or even an increase in yield. In contrast, summer crops show a remarkable decrease of yield. This different pattern is attributed to a lengthier drought period during summer and to an increased rainfall in winter and autumn. Regarding forest fire risk, an additional month of risk is expected over a great part of the basin. Energy demand levels are expected to fall significantly during a warmer winter period inland, whereas they seem to substantially increase nearly everywhere during summer. Extremely high summer temperatures in the Mediterranean, coupled with improved climate conditions in northern Europe, may lead to a gradual decrease in summer tourism in the Mediterranean, but an increase in spring and autumn.

1. Introduction

The global warming predicted by climate models for the 21st century is a threat to most natural systems at every latitude and region. Since its implications are characterised by strong latitudinal variations (IPCC, 2001a, 2007), regional studies are proving to be an essential tool for scientists and decision-makers. The present paper investigates climate changes and associated sectoral impacts in the Mediterranean at the time of 2 °C global warming. A global mean temperature change of 2 °C is considered to be a critical level beyond which dangerous climate change occurs. For rising temperatures beyond 2 °C, increasing risks of extreme events, distribution of climate impacts or aggregated effects on markets are becoming a growing reason for concern (Smith et al., 2001). In addition, strong positive carbon cycle feedbacks are increasingly likely (Friedlingstein et al., 2003; Jones et al., 2003a,b), which would lead to even more climate change beyond the direct effect of anthropogenic emissions.

While observations limit climatic analyses to local scales (e.g. Fontaine et al., 1999; Founda et al., 2004), this deficiency was overcome by climate models, which provide data on a wide range of temporal and spatial scales. Regionalization of global models has been performed by three different techniques over the last decade. Statistical downscaling has been applied (Wilby et al., 1998), high-resolution "time-slice" atmospheric general circulation models (Gibelin and Déqué, 2003; Giorgi and Bi, 2005) and most recently nested regional climate models (Gao et al., 2006) have been developed. However, up to date, they have all focused on the 2071–2100 period as can be seen in the recent EU-funded projects PRUDENCE (Christensen et al., 2002; Räisänen et al., 2003; Giorgi et al., 2004; Deque et al., 2005) and MICE (Hanson et al., 2007), or they focus on an indeterminate period when a doubling of CO_2 concentration occurs (Giorgi et al., 1992; Jones et al., 1997; Déqué et al., 1998). Efforts to overcome this temporal

* Corresponding author. Tel.: +30 210 8109128; fax: +30 210 8103236.
E-mail address: cgiannak@meteo.noa.gr (C. Giannakopoulos).

0921-8181/$ – see front matter © 2009 Elsevier B.V. All rights reserved.
doi:10.1016/j.gloplacha.2009.06.001

limitation are underway through the European FP6 ENSEMBLES project (http://ensembles-eu.metoffice.com).

The closer time of a 2 °C global warming deserves attention, since a general drying has already been detected over most of the Mediterranean (IPCC, 2001b; Giorgi, 2006; Gao and Giorgi, 2008). The region's sensitivity to drought and rising temperature are of prime interest for agriculture, tourism, water resources and policy makers. Summer temperatures are likely to increase by more than 2 °C, with a corresponding increase in the frequency of occurrence of severe heatwaves (Diffenbaugh et al., 2007). The 2003 heatwave in Europe (Beniston, 2004; Schär et al., 2004) has dramatically illustrated the need to provide projections of climate change for a time period earlier than 2070. Such a study has been performed by New (2005) for the Arctic. This might be beneficial mainly to stakeholders, policy makers and impacts people since they require shorter timescales for their policy planning ahead.

Since the time of a 2 °C global warming is expected between 2026 and 2060 (Section 2), at the time of the experimental runs for this paper, only General Circulation Models (GCMs) were available to assess the climatic characteristics in the Mediterranean during this period. Although GCMs present a range of sensitivity to greenhouse gas and aerosol forcing, which in turn depends on emission scenarios for future estimates, only data from one model, the HadCM3, have been used in the present study. As discussed in Section 2, the results are representative of the currently available global climate models for the considered time period. Climatic changes are determined through comparison between control (1961–1990) and future (2031–2060) years. Means and extremes are used to describe future changes. Seasonal and yearly parameters are considered. The confidence in the estimated changes for each parameter is important and determined with the bootstrap method.

2. Method and the 2 °C global warming

2.1. Climate model data and the 2 °C warming

New (2005) carefully addresses the time of 2 °C global warming predicted by GCMs. Considering 21 climate change simulations from six GCMs and four IPCC emissions forcing scenarios, series of global mean temperature-anomalies, defined as difference with pre-industrial value, have been calculated. The time of 2 °C global warming found by New (2005) is between 2026 and 2060, depending on the sensitivity of the model to greenhouse gas forcing and to future scenarios. The various series are reproduced in Fig. 1. Model comparison studies

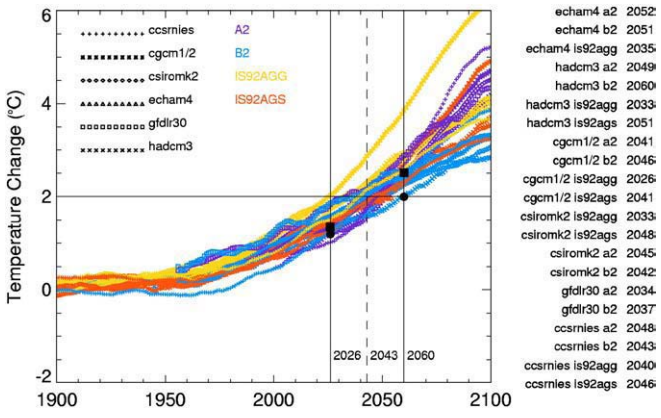

Fig. 1. Global mean annual temperature anomalies relative to control climatology, smoothed with a 21-year moving average. Vertical lines indicate the range in time at which the 21-year global mean temperature anomaly exceeds +2 °C. The two black circles (squares) indicate the HadCM3-A2 (B2) temperature at this range limits. Numbers on the right show the time at which the 21-year mean global temperature anomaly exceeds +2 °C for each GCM-scenario combination. (adapted from New (2005)).

have shown that results from different models for the 2026–2060 period agree with one another fairly well, while most of the divergence takes place in the latter part of the century (2070–2100) (IPCC, 2001b). The same conclusion is drawn from Fig. 1, particularly if the outlier series cgcm1/2 IS92aGG (scenario with greenhouse gas only) is disregarded. The range of simulation results starts to really spread after 2060. To study the 2026–2060 period, considering 20 simulations, or just one with an average response, to forcing scenarios will give similar results although spatial differences may still be present among models. The advantage of using one model resides in the knowledge of its weaknesses and shortcomings, which can prove important in interpreting results.

In the present study, output from the HadCM3 model (Gordon et al., 2000; Pope et al., 2000) driven by SRES A2 and SRES B2 scenarios are used. The model couples an atmospheric GCM to an ocean GCM. Unlike earlier atmosphere–ocean GCMs, flux adjustment (i.e., additional artificial heat and freshwater fluxes at the ocean surface) is not required to produce a simulation. The high ocean resolution of HadCM3 is a key factor in this improvement. The atmospheric component of HadCM3 has 19 levels with a horizontal resolution of 2.5° of latitude by 3.75° of longitude, which produces a global grid of 96 by 73 grid cells. This is equivalent to a surface resolution of about 417 km by 278 km at the Equator, reducing to 295 km by 278 km at 45° of latitude (comparable to a spectral resolution of T42). Hence, the model geography is much simpler than the real-world geography. As an example, only two grid cells cover Greece, one land (northern Greece) and one sea (southern Greece) grid cell. When discussion is made about coastal areas in the text, reference is made to the model coast areas (transition areas between land and sea grid boxes), which may not fully coincide with real coast areas. Panel 1 displays the land–sea mask of HadCM3 over the Mediterranean. The oceanic component of HadCM3 has 20 levels with a horizontal resolution of 1.25 by 1.25°. At this resolution it is possible to represent important details in oceanic current structures. Mediterranean water is partially mixed with Atlantic water across the Strait of Gibraltar as a simple representation of water mass exchange, since the channel is not resolved in the model.

HadCM3 has been run for over a thousand years, showing little drift in its surface climate. The control run is basically the GCM being run for 240 years at 1961–1990 atmospheric concentrations. Any variation in the control run should stem from natural variability. The last 30 years of the control run, 1961–1990, are used here as reference for comparison with future predictions. The control run is unforced and thus common to any scenario that may apply after 1990. Here we considered the A2 and B2 emissions scenarios. These depend on several drivers such as population growth, economic and technological development, natural resources etc (Nakicenovic et al., 2000). With a population of 15 billion by 2100, the A2 world undergoes a greater rate of warming than the B2 world with its medium 10.4 billion population projection and its focus on local solutions to economic, social and environmental sustainability.

Indication of HadCM3 average response to forcing scenarios is provided by its transient climate response (TCR). The TCR is commonly used to compare model responses to a same standardised forcing. The TCR of HadCM3 is 2 °C, which occupies an average position within the range of TCRs (1.4 °C–3.1 °C) of the 19 GCMs assessed in the IPCC Third Assessment Report (IPCC, 2001b). Characteristics for both scenarios are shown in Fig. 1. A pair of black squares (circles) indicates the temperature anomaly according to HadCM3 under A2 (B2) scenario in 2026 and 2060. The HadCM3 clearly exhibits an average response for A2 and a conservative one for B2, with respect to the time of 2 °C global warming between 2049 and 2060. Regarding changes in climatic means and extreme values, results from both scenarios are so similar for the period considered here that they are collected together to improve their confidence levels (see Section 3).

Based on daily model outputs, each annual parameter (an extreme, a mean or accumulated value) is computed and averaged over future

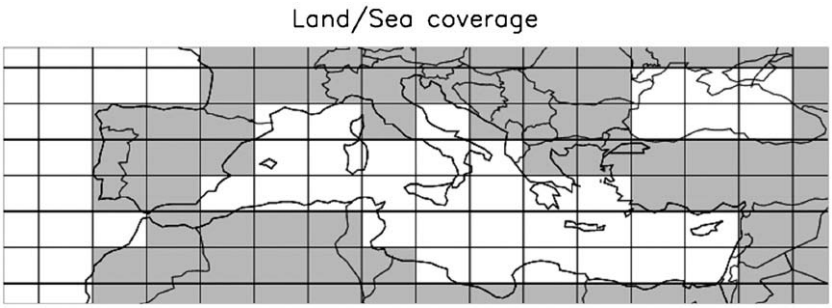

Panel 1. Land–sea mask of HadCM3 over the Mediterranean. The squares represent the size of the HadCM3 grid cell. Grey colour denotes land and white denotes sea as represented in the model.

(2031–2060) and control (1961–1990) years. Note that the 2026–2060 period of Section 2 is reduced to 2031–2060, because the same number of years is required to bootstrap the differences. The difference between both averages is examined using a confidence estimate. With respect to the difference, the control period is subtracted from the future, except in one instance clearly noted below. Thus positive values indicate an increase in the future. The confidence in estimated changes is obtained by bootstrapping (Mudelsee and Alkio, 2007) the differences between the two periods. The method resamples the annual difference parameter 1000 times with replacement and calculates the mean of each sample. The 95-percentile confidence limits are computed based on the resulting series. In the resampling process, each sample consists of 30 values.

In our study, A2 and B2 scenario simulation results are considered together, so that the sample population is doubled to 60 and confidence limits are higher. The procedure mentioned above is repeated to get A2/B2 average results and this method (difference, bootstrapping, and A2/B2 averages) is applied to all studies that follow.

2.2. Impact models

2.2.1. Crop productivity

CROPSYST model (Cropping Systems Simulation Model) (Stockle et al., 2003) and HadCM3 data (*T*min, *T*max, rainfall and global radiation) were used for simulating crop productivity under the selected present and future climate scenarios.

CROPSYST is a multi-year, multi-crop, daily time-step crop growth simulation model, which simulates the soil water budget, the soil–plant nitrogen budget, crop canopy and root growth, crop phenology, dry matter production, yield, residue production and decomposition, and erosion. The model allows the user to specify management parameters such as sowing date, cultivar genetic coefficients, soil profile properties, fertilizer and irrigation management, tillage and atmospheric CO_2 concentration. As for most crop simulation models, CROPSYST does not include the direct effect of extreme temperatures on crop development and growth, thus only changes in mean climate conditions are considered to affect crop yields.

HadCM3 data for hotspot cells were selected to provide a homogenous cover of Mediterranean basin and to study the areas where changes in precipitation and temperature patterns are expected to be substantial, according to HadCM3 model simulations. More specifically 13 grid cells (called 'hot spots') of the HadCM3 have been selected (Panel 2).

For each hotspot, five types of agricultural crops, having different characteristics based on i) photosynthesis pattern (C3 and C4 crops), ii) growing period (winter and summer seasons), iii) food composition (protein, e.g. legumes and carbohydrates, e.g. tuber crops), were selected on the basis of their relative importance (Table 1), as have been reported in the FAOSTAT database (http://faostat.fao.org/).

At first, CROPSYST model was calibrated to fit as much as possible the data reported on the FAOSTAT database (http://faostat.fao.org/). The calibration showed that CROPSYST outputs match quite closely with the statistical crop productivity data collected by FAO, with mean absolute errors ranging from 1% to 14%. Next, for each 'hot spot' and crop type the annual values of development stages and yields were calculated for the two time-slices (1961–1990 and 2031–2060). In particular, for the present climate the simulation runs were done setting the atmospheric concentration of CO_2 at 350 ppm; whilst the simulation runs for the future climate scenarios were performed with increasing CO_2 (470 ppm under scenario B2 and 520 ppm under scenario A2). Accordingly, crop responses (e.g. changes in radiation and water use efficiencies) under elevated CO_2 were set on the basis of metadata analyses made by Kimball et al. (2002), Ainsworth and Long (2005). Finally, the CROPSYST model was rerun introducing

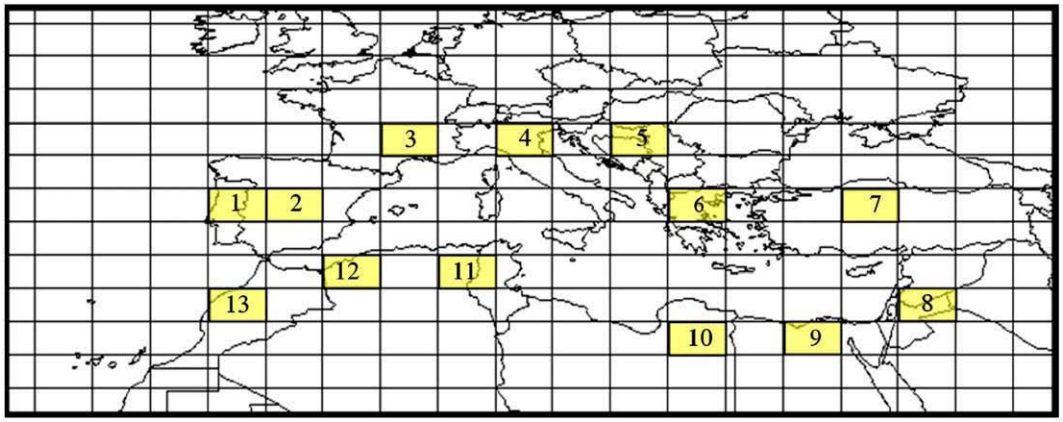

Panel 2. Grid cells of Had CM3 selected for the impact assessment on agriculture.

Table 1
Type of crop simulated in each of the selected grid cell.

Grid cell number	Country	C4 summer crop	C3 summer crop	Legumes	Tuber crops	Cereals
1	Portugal	Maize	Sunflower	Bean	Potato	Wheat
2	Spain	Maize	Sunflower	Lentil	Potato	Barley
3	France	Maize	Sunflower	Soybean	Potato	Wheat
4	Italy	Maize	Sunflower	Soybean	Potato	Wheat
5	Serbia	Maize	Sunflower	Soybean	Potato	Wheat
6	Greece	Maize	Sunflower	Bean	Potato	Wheat
7	Turkey	Maize	Sunflower	Lentil	Potato	Wheat
8	Jordan	Maize	Sunflower	Lentil	Potato	Barley
9	Egypt	Maize	Sunflower	Bean	Potato	Wheat
10	Libya	Maize	Sunflower	Bean	Potato	Wheat
11	Tunisia	Maize	Sunflower	Bean	Potato	Wheat
12	Algeria	Maize	Sunflower	Bean	Potato	Wheat
13	Morocco	Maize	Sunflower	Bean	Potato	Wheat

adaptation management strategies (e.g. changes in sowing dates, cultivar, etc.) that may reduce the negative impact of climate change or enhance positive impacts. In all simulations, the C4 summer crops and tuber crops were considered as "irrigated crops", whereas the rest of the crops were considered as "rain-fed crops". Nitrogen was considered not limiting for all the crops.

2.2.2. Energy demand

Energy demand is linked to climatic conditions (Giannakopoulos and Psiloglou, 2006) and the relationship of energy demand and temperature is non-linear. The variability of ambient air temperature is closely linked to energy consumption, whose maximum values correlate with the extreme values of air temperature (maximum or minimum). In the Mediterranean region, during January, the maximum values of energy consumption are related to the appearance of the lowest temperatures. During the transient season of March–April, energy consumption levels are kept nearly constant until about May, while air temperatures are constantly rising. From mid-May onwards, and throughout the summer period, any increase in air temperature corresponds to an increase in energy consumption mainly due to the extensive use of air conditioning systems. An exception is found for August when most local people tend to take their summer holidays, and hence the demand for air conditioning is reduced especially in large Mediterranean cities. Another transient period exists during September and October where energy demand and consumption are kept at constant levels. This transient period is followed by a period of continually increasing energy demand with a peak before the Christmas festive period. Therefore, it is anticipated that warmer climate conditions will lead to decreased demand in winter, while increased demand should be typical during summer time (Valor et al., 2001; Giannakopoulos and Psiloglou, 2006). Moreover, the effect of higher temperatures in summer is likely to be considerably larger on peak energy demand than on net demand, suggesting that there will be a need to install additional generating capacity over and above that needed to cater for underlying economic growth.

Since the energy–temperature relationship is non-linear and has two branches, it would be more convenient to separate these two branches. The easiest way to achieve this is to use the idea of Degree-Day, which is defined as the difference of mean daily temperature from a base temperature. Base temperature should be the temperature where energy consumption is at its minimum. If this temperature is chosen, then the degree-day index is positive in the summer branch and negative in the winter branch. Instead of having both positive and negative values for this index, the definition of two indices is used: heating (HDD) and cooling degree days (CDD).

For the calculation of the HDD and CDD indices, the following equations were used:

$$\mathrm{HDD} = \max(T^* - T, 0) \quad (1)$$

$$\mathrm{CDD} = \max(T - T^{**}, 0) \quad (2)$$

where T^* and T^{**} are the base temperatures for HDD and CDD respectively, which can be either the same or different and T is the

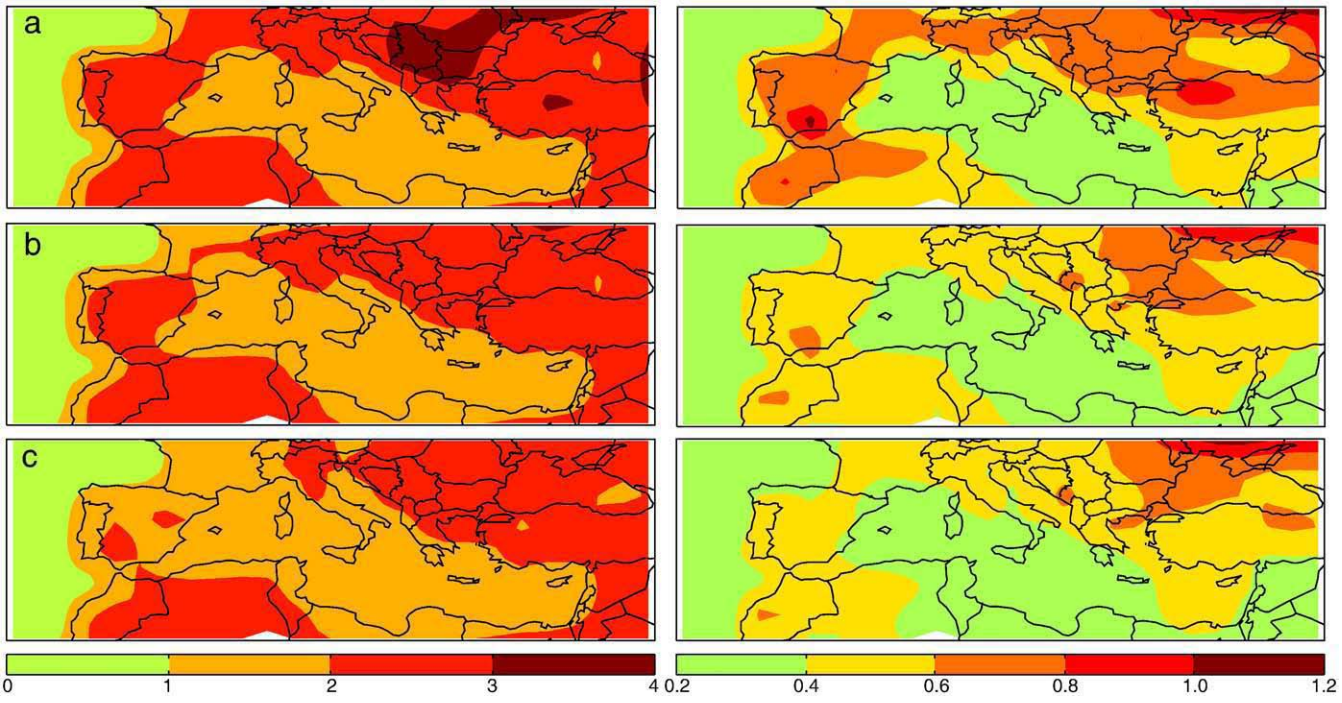

Fig. 2. Left column: difference in the average annual (a) maximum, (b) mean, and (c) minimum temperature (°C) between 2031–2060 and 1961–1990. Right column: the corresponding 95% confidence range.

mean daily temperature calculated from the daily data of HadCM3 for both the reference and the future periods.

HDD (CDD) is a measure of the severity of winter (summer) conditions in terms of the outdoor dry-bulb air temperature, an indication of the sensible heating (cooling) requirements for the particular location. Kadioğlu et al. (2001) used different base levels of 15 °C and 24 °C for the calculations of HDD and CDD respectively in Turkey. In our study we use 15 °C for the calculation of HDDs and 25 °C for the calculation of CDDs. We identify the changes in energy demand levels by showing differences in the cumulative numbers of CDDs and HDDs between the reference and the future period.

2.2.3. Forest fire risk

One of the potential detrimental impacts of anthropogenic climate change is increased wildfire occurrence. Mediterranean Europe, in particular, has been identified as likely to suffer potentially increased fire risk (Pinol et al., 1998; Moriondo et al., 2006). The contribution of meteorological factors to fire risk is simulated using various non-dimensional indices of fire risk. Viegas et al. (1999) validated a number of fire indices in the Mediterranean against observed fire occurrence, and the Canadian Fire Weather Index (FWI, van Wagner, 1987) was among the best performers. Viegas et al. (2001) demonstrated that in summer, the slow response of live fine fuel moisture content to meteorological conditions is well described by the Drought Code subcomponent of the FWI system. In addition, FWI is one of the most widely used indices of fire risk. Therefore, output from climate model simulations of the coming decades was used to the FWI model to examine potential changes in Mediterranean fire.

The Canadian Fire Weather Index system is described in detail in van Wagner (1987). Briefly, it consists of six components that account for the effects of fuel moisture and wind on fire behaviour. These include numeric ratings of the moisture content of litter and other fine fuels, the average moisture content of loosely compacted organic layers of moderate depth, and the average moisture content of deep, compact organic layers. The remaining components are fire behaviour indices, which represent the rate of fire spread, the fuel available for combustion, and the frontal fire intensity; their values rise as the fire danger increases. Fire risk is low for FWI<15, and increases more rapidly with FWI>15 (Good et al., 2008). A threshold of FWI>30 was selected as a measure of increased fire risk.

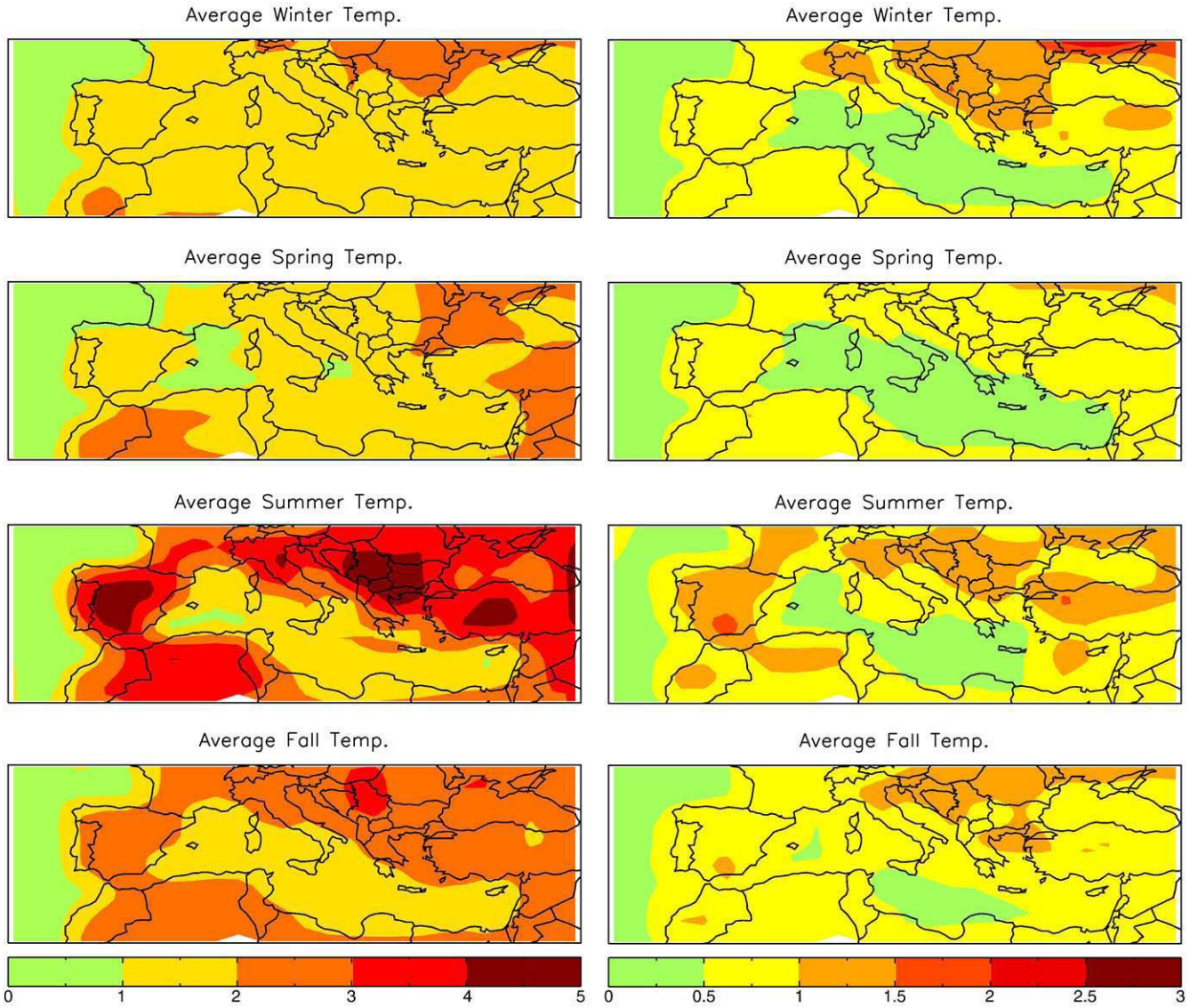

Fig. 3. Left column: difference in mean (a) winter, (b) spring, (c) summer and (d) autumn temperatures between 2031–2060 and 1961–1990. Right column: the corresponding 95% confidence range.

3. Changes in climate

3.1. Temperature changes

The Mediterranean basin will experience an average 2 °C warming at the same time as the average globe. Because of the latitudinal variation in the amount of warming at the time of a 2 °C global warming, we first look at changes in annual mean temperatures. The left column of Fig. 2 shows maps of changes in annual mean of daily maximum (*T*max), mean (*T*mean) and minimum (*T*min) temperatures. The confidence range in the right column is the difference between the upper and lower confidence limits. It is mainly a practical way to present these limits into one plot. Dividing the confidence range by two gives the value to add or subtract from the mean difference in the left column to get the limits. For example, we are 95% confident that the rise in *T*mean along the Mediterranean rim will be between 1.8 and 2.2 °C (2 °C ± 0.2 °C). This is a 10% uncertainty in the prediction. Due to the thermal inertia of the Mediterranean Sea, the daily mean temperature rise (Fig. 2b) is between 1–2 °C (± 0.15) along the coast, and 2–3 °C inland (± 0.25). It is slightly larger in daytime (Fig. 2a), exceeding + 3 °C in the Balkans. In the south of France and the Iberian Peninsula, the rise is slightly lower at night (Fig. 2c).

Seasonal changes, shown in Fig. 3 for the daily mean, are more pronounced, and have more uncertainty. The rise occurs mainly in summer (Jun/Jul/Aug), when it reaches 4 °C inland on average. It rises above this value in the Balkans, Turkey, north Italy, and Spain, with a confidence of about ± 0.75 °C (18%). Autumn (Sep/Oct/Nov) has the second largest warming in absolute terms: mean temperatures rise above 2 °C (± 18%). Winter (Dec/Jan/Feb) is likely to be warmer by 1–2 °C with an uncertainty of 25% (± 0.25–0.5 °C). Spring (Mar/Apr/May) has a very similar pattern, but with slightly more warming in the Asian side. Since *T*max and *T*min present the same seasonal variations as *T*mean, they are not shown here. However, a smaller summer increase at night (*T*min) and a larger daytime increase (*T*max), both by about 1 °C, are found inland but not along the coast.

Better insight into the future Mediterranean climate can be gathered from extreme values of temperature. We have chosen indices of extremes with fixed thresholds appropriate for the Mediterranean

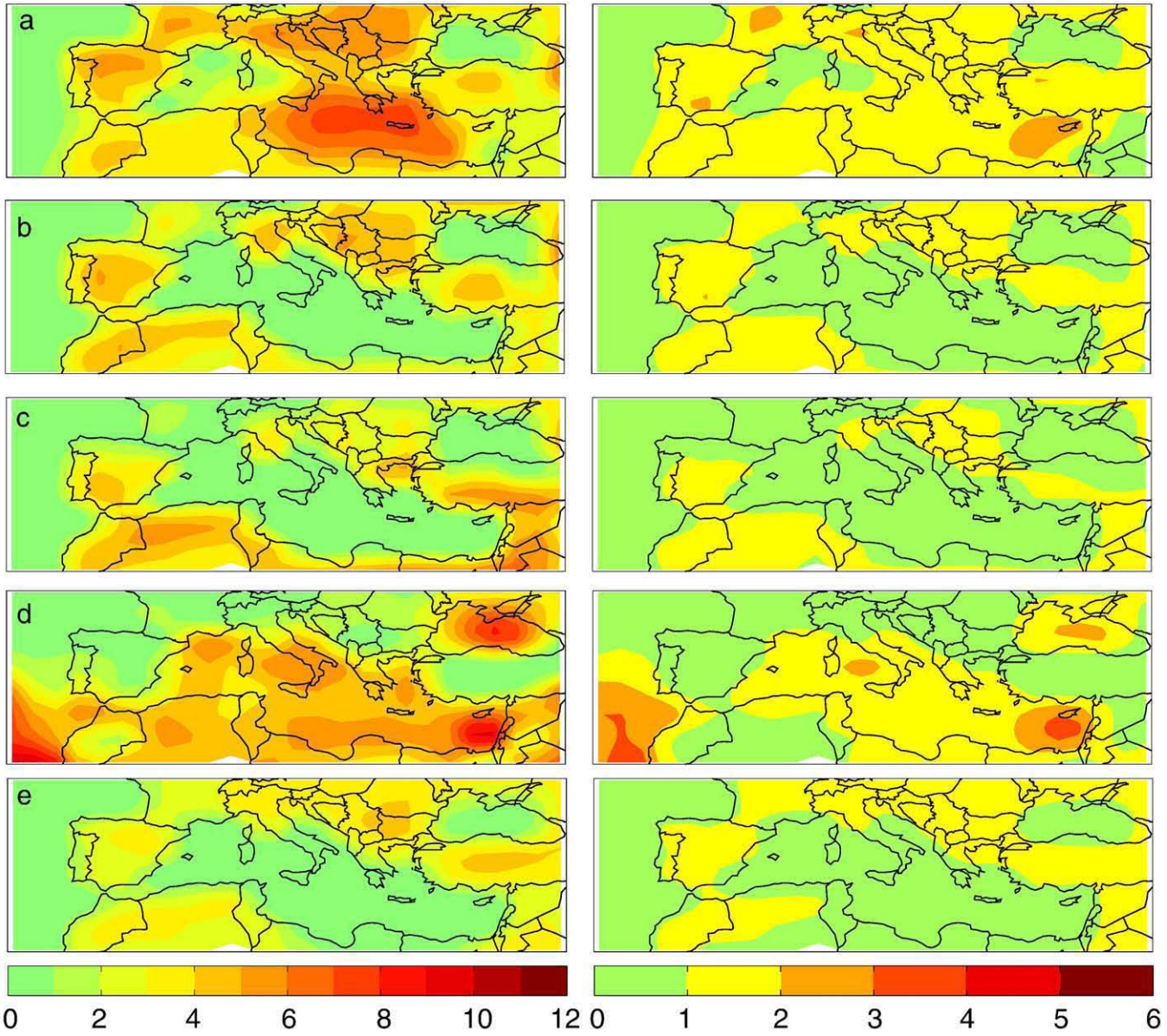

Fig. 4. Left column: increase in the number of (a) summer days, (b) hot days, (c) heatwave days, and (d) tropical nights, and (e) decrease in the number of frost nights between 2031–2060 and 1961–1990. Averaged annual numbers are considered and units are weeks. Right column: the corresponding 95% confidence range in weeks.

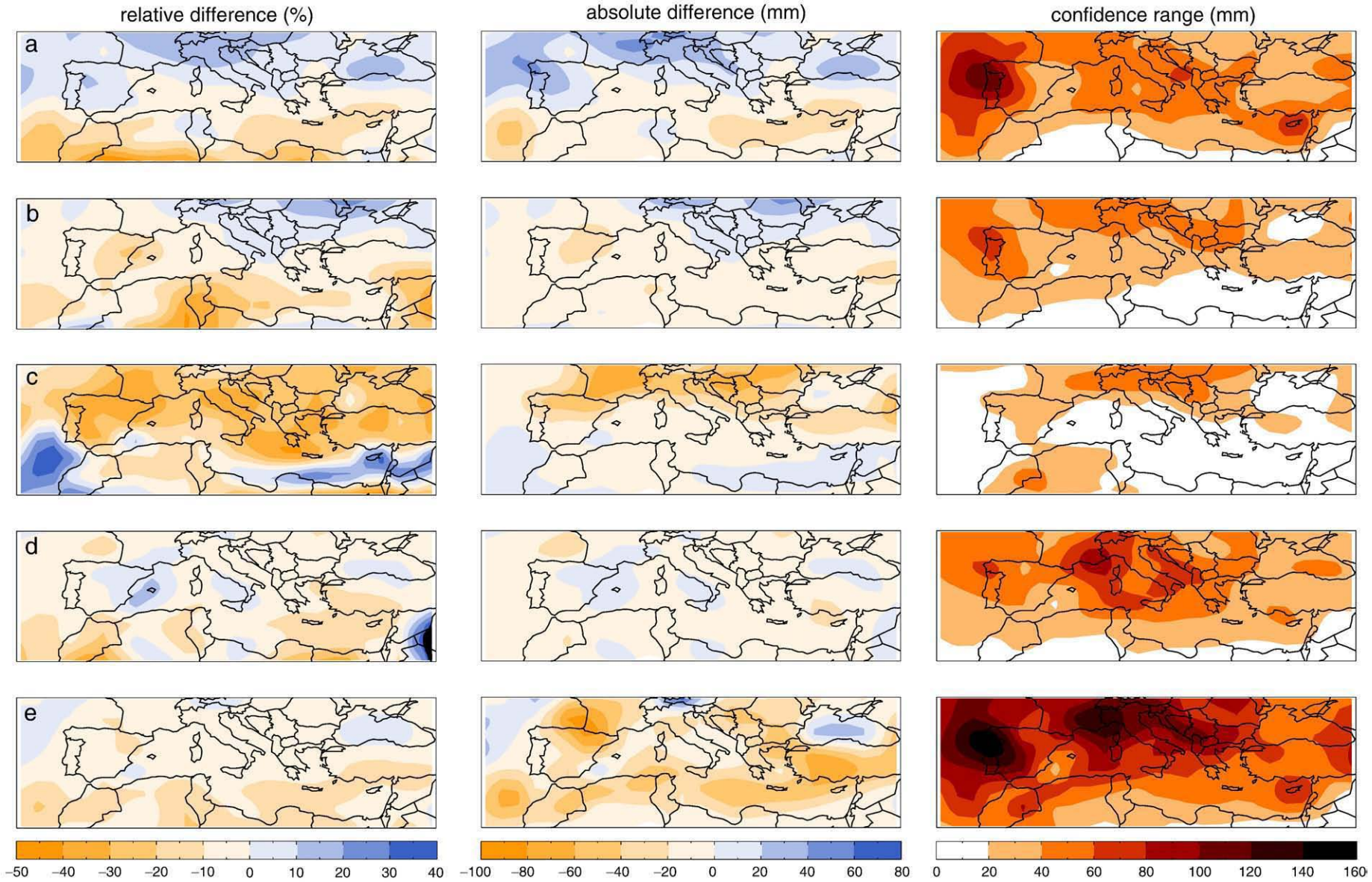

Fig. 5. Left column: percentage changes in annual rainfall accumulated over (a) winter, (b) spring, (c) summer, (d) autumn, and (e) the full year between 2031–2060 and 1961–1990. Centre column: same as left column but for absolute changes. Right column: the corresponding 95% confidence range. Units are in mm.

climate as fixed threshold values are more appropriate for an area with similar climatic characteristics and are easier for impacts people to understand and use. The following annual indices of temperature extremes have been calculated:

- Number of summer days (Fig. 4a), defined by *T*max>25 °C.
- Number of hot days (Fig. 4b), defined by *T*max>30 °C.
- Number of heatwave days (Fig. 4c), defined by *T*max>35 °C.
- Number of tropical nights (Fig. 4d), defined by *T*min>20 °C.
- Number of frost nights (Fig. 4e), defined by *T*min<0 °C.

Note that units are in weeks, and the convention used in this paper is exceptionally broken in Fig. 4e, where the difference between both periods is obtained by subtracting the future period from the control. The largest increases are found in summer days and tropical nights at coastal areas, especially in the East part of the Mediterranean). These indices (Fig. 4a and d) are moderate extremes. The Mediterranean Sea does not temper their increase, as opposed to the more extreme indices (Fig. 4b, c, and e).

Overall, about one additional month of summer days is expected (Fig. 4a). Summer days increase more in the milder northern part of the basin, up to 6 (±1) weeks inland, and less in the Maghreb and the land areas to the easternmost of the region. The longer summers are accompanied by additional tropical nights (Fig. 4d), again along the coasts. However, the north/south dichotomy is inverted: the increase mainly affects land areas of the Southern Mediterranean, while lots of nights in the northern part remain below the 20 °C threshold, despite the night-time warming (Fig. 2d). To summarise, we have defined two distinct land regions:

- the northern with more than a month of summer and half a month of tropical nights,
- the southern and easternmost part with about one extra month of summer and more than a month of tropical nights

Increases in the number of hot (Fig. 4b) and heatwave (Fig. 4c) days, as well as decrease in the number of frost nights (Fig. 4e), have a similar spatial pattern with slightly different magnitudes depending on the location. Increases range from 2 weeks (±0.5) along the coasts to about a month (±0.5–1 week) inland. Owing to its proximity to the Atlantic Ocean, only one land grid cell runs across the Pyrenean chain, and hence the south of France appears less sensitive to high extreme changes. On the contrary, three model land grid cells separate the ocean from the sea across the Iberian Peninsula, where the ocean proximity is not felt in extreme indices.

3.2. Precipitation changes

The second part of the study focuses on the precipitation regime. As shown in Fig. 5e (centre), annual total rainfalls mainly decrease. The spatial variation (Fig. 5e-left) is relatively small. It is less than 10% in the major part of the Basin, and between 10 and 20% in the already drier southern part. Uncertainties (Fig. 5e-right) are a lot larger than for temperature changes. They are above ±50% of the expected change everywhere (Pyrenees and southern Turkey are the only exception with an uncertainty between 25 and 50%). They are roughly in the 75–150% range where the future changes are significant (~ >20 mm). These large uncertainties might stem from large intra- and inter-annual variabilities. The intra-annual variability can be perceived in seasonal variations pictured in Fig. 5a–d and discussed below. The inter-annual variability of precipitation is well known (Bolle, 2003; Lionello et al., 2006) and reproduced in the simulations.

The difference between emission scenarios does not significantly contribute to the uncertainties. The largest differences between A2 and B2 are found over Portugal. The B2 scenario predicts some increase (occurring mainly in winter), while A2 predicts a decrease in precipitation. However, both cases include huge uncertainties in these areas (above ±200%). The uncertainty associated with Portugal in Fig. 5e (right) is only due to intra- and inter-annual variability. In other words, the differences between the two scenarios are not statistically significant when other uncertainties are taken into account. Finally, better confidence is gained by piecing together the two simulation results.

The picture of a globally drier Mediterranean Basin conceals seasonal variability as shown in Fig. 5a–d. The main features are the winter and summer changes in the north of the Basin. The latter becomes wetter in winter (about +10%), but this is largely compensated by a drier summer (−30%). Autumn (Fig. 5d) is the season with the fewer changes. On the other hand, the southern Mediterranean is projected to endure an almost evenly distributed small decrease in precipitation all year round. Note that the drier north is the most reliable expectation with less than ±50% uncertainty. Autumn reveals the largest uncertainty that rises above 200% in most of the area, but the changes are small in absolute terms. In summary, a globally 10% drier Mediterranean region is expected.

Further insight is gathered in investigating the number of dry days and spells, and the annual maximum running total rainfall over 3 days. We have chosen the three-day total in order to catch the total rain amount accumulated over this short time period that may have the

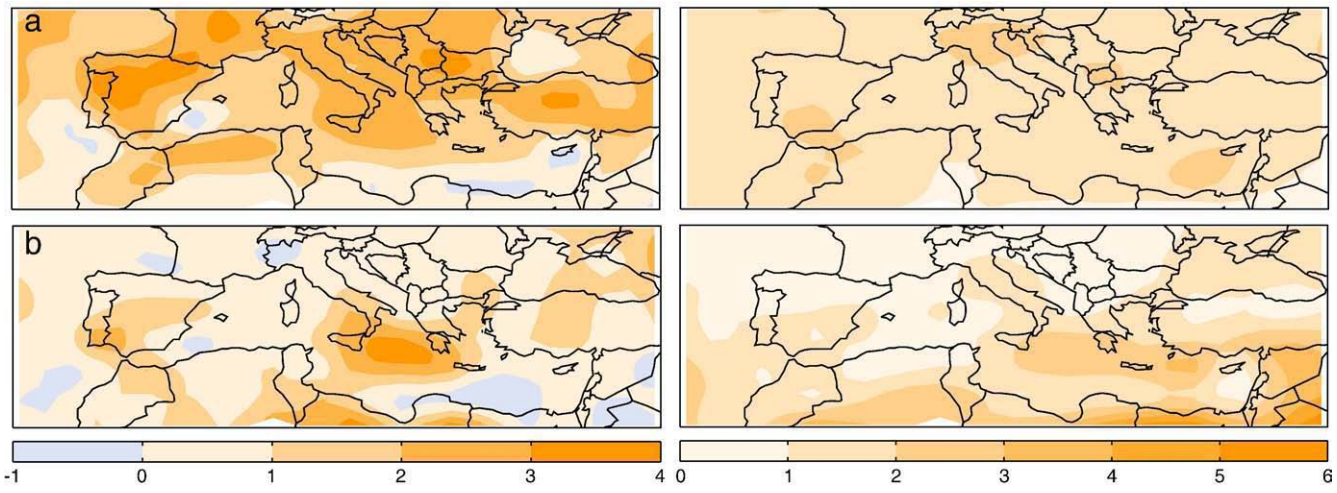

Fig. 6. Left column: differences in annual (a) number of dry days and (b) length of longest dry spell averaged over 2031–2060 and over 1961–1990, in weeks. Right column: the corresponding 95% confidence range in weeks.

potential to cause localised flooding. Days are qualified as dry if daily precipitation (RR) amounts to less than 0.5 mm, a typical threshold value in modelling studies (Hanson et al., 2007). The change in the number of these days is shown in Fig. 6a (units are in weeks). The 2 °C global warming is characterised by 1–3 weeks (±5 days) of additional dry days. The spatial pattern follows the temperature increase with smaller changes (~1 week) in the already dry southeast basin and along the coast, and larger ones inland. The Iberian Peninsula, the Balkans, Turkey and the south of France feature the largest increases (above 3 weeks).

Similar results are obtained if the daily precipitation threshold is raised to 1 mm. The number of wet days (RR>10 mm) and very wet days (RR>20 mm) feature ±3 days of change for the former and none for the latter. We conclude that the increase of dry days is concomitant to a decrease of rainy days (not shown) within the 1–10 mm RR range. Not surprisingly, the longest wet spells show little change in their length. However, the longest droughts (Fig. 6b) lengthen by about a week. It is worth noting that the spatial pattern of droughts is similar to the pattern of the increase in summer days (Fig. 4a).

Although they are not strictly extreme indices, the average shifts of start (Fig. 7a) and end (Fig. 7b) of the longest drought are worth examining, because of their interest for agriculture and the tourism industry. In Fig. 7, a positive value means a shift toward the year-end. The general tendency is a small shift (slightly larger under B2 than A2 scenario) towards autumn, with the exception of the south of France and inland Algeria where the longest droughts start and end 2 weeks earlier on average. These estimates are associated with a ±1 week uncertainty. The annual maximum running total rainfall over 3 days is an extreme index, shown in Fig. 8. The rain intensification seen on the northern half is a direct consequence of precipitation increase during winter (Fig. 5a). On the contrary, the steady small precipitation decrease all year long in the southern half leads to lower highest accumulated rainfall. The uncertainties range between ±100%.

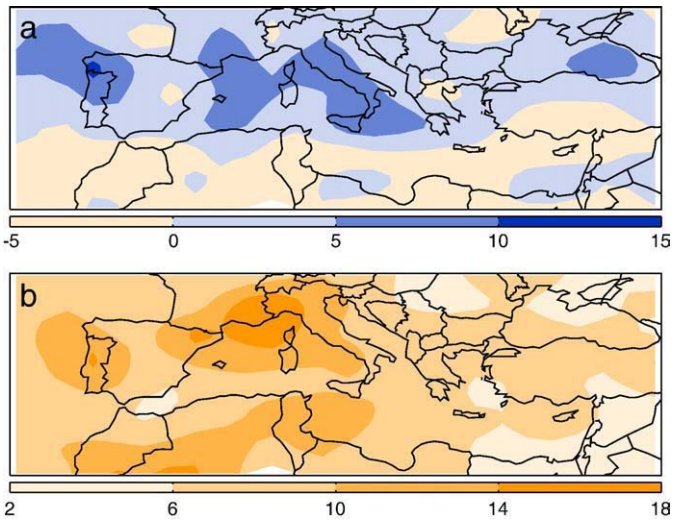

Fig. 8. Top: averaged difference in annual maximum running total rainfall over 3 days between 2031–2060 and 1961–1990 in mm. Bottom: corresponding 95% confidence range.

4. Impact assessment

4.1. Crop productivity

The results of the CROPSYST simulation run for the different crop types and for the present and future climate scenarios are summarised in Fig. 9. The irrigated crops considered in this study (i.e. summer C4 and tuber crops), showed a prevalent reduction of yield in the hot spots located in the African and Asian Mediterranean countries whereas in the European hot spots, yields showed a consistent increase.

The yield of rainfed crops sown in spring was generally depressed by a warmer and drier climate over the entire basin, with a few exceptions. Legumes showed a general reduction of yield in all the hot spots with the exception of those on Spain, Turkey and Greece. C3 summer crops showed a general reduction of yields in the hot spots located on northern and southwestern parts of the Mediterranean basin, whereas in those located in the southern or eastern parts, yields remained unchanged. By contrast, cereals presented a prevalent increase in yields, which was more evident in the southern and eastern parts.

In summary, the effect of climate change on agriculture is likely to be more severe in the southern Mediterranean areas than in the northern temperate areas. In the warmer southern Mediterranean, increases in CO_2 help reduce the loss in yield arising from a warmer and drier climate, but are not able to completely recover the losses. In the cooler northeastern Mediterranean, CO_2 increases associated with climate change result in little net effect on most crops, provided that the increase in water demands, especially for irrigated crops, can be met (Table 2).

Introduction of adaptation strategies to cope with impacts of global change show that early sowing date associated with the shortening of growing season (due to high temperatures) may reduce the negative impacts of climate change or even enhance positive impacts allowing

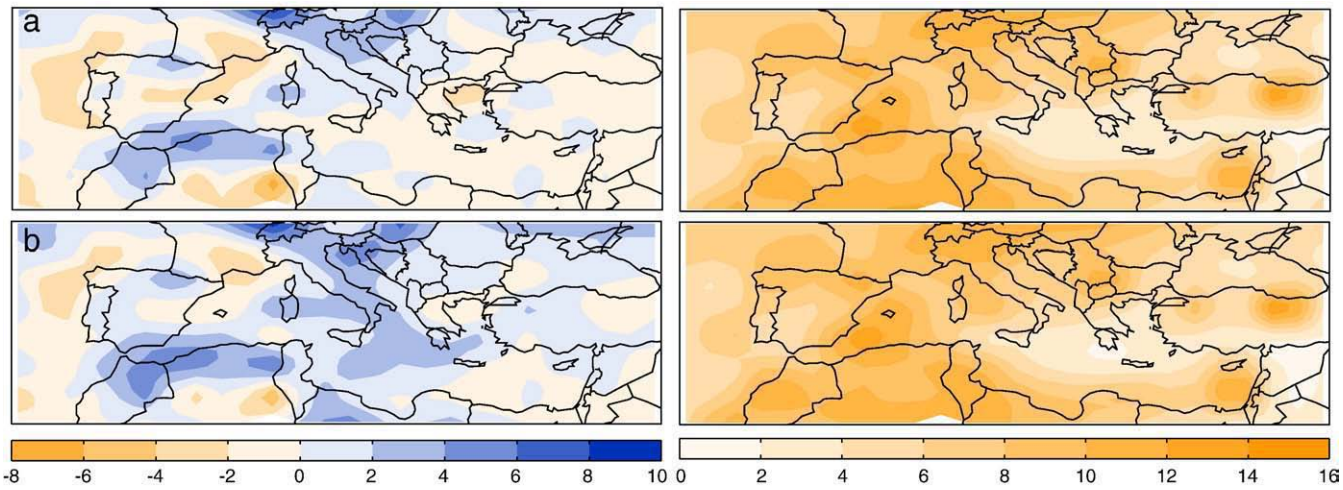

Fig. 7. Averaged shift of (a) start and (b) end of the longest dry spell between 2031–2060 and 1961–1990, in weeks. Right: corresponding 95% confidence range.

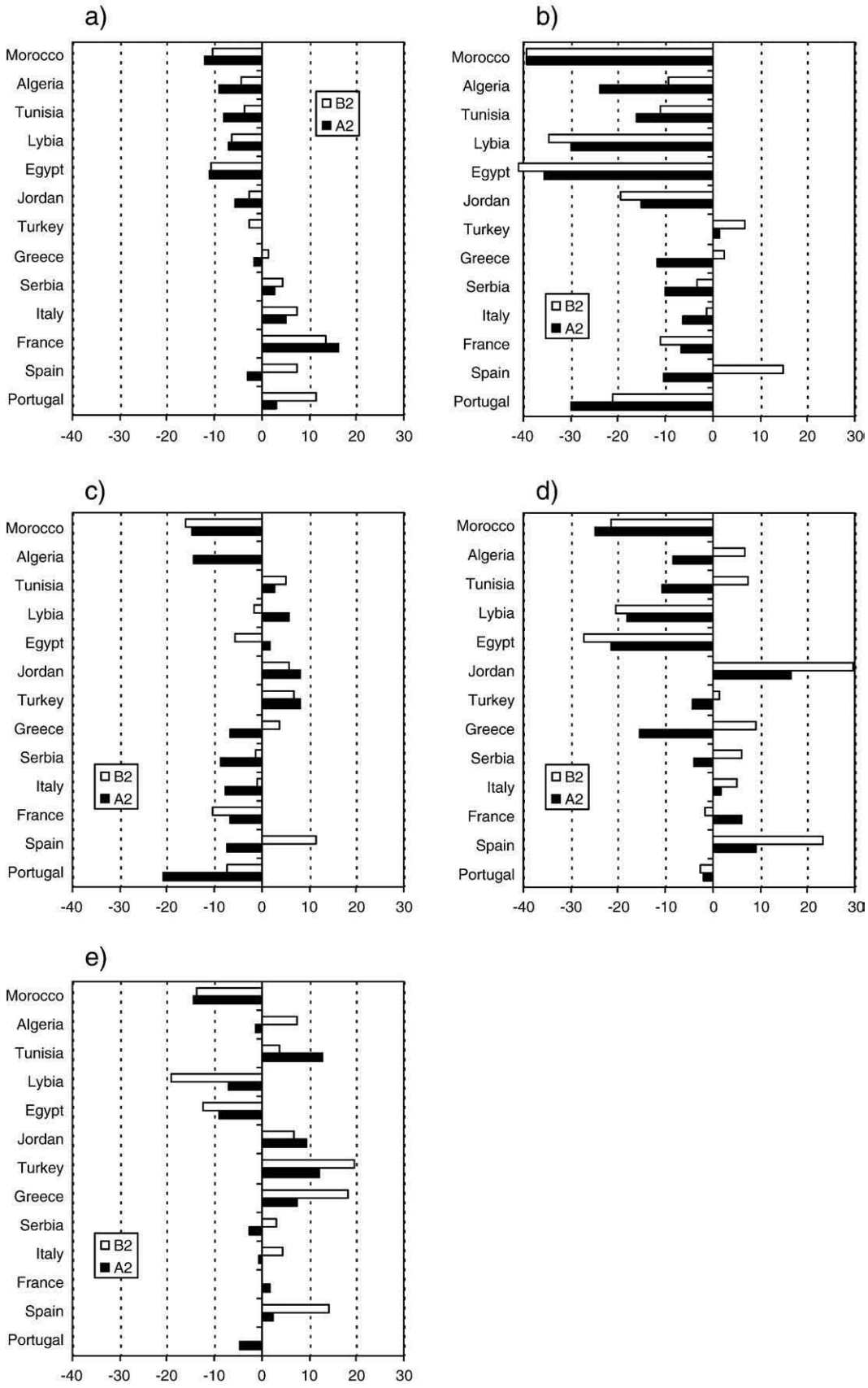

Fig. 9. Impact of climate change on crop productivity for: a) C4 summer crop, b) legumes, c) C3 summer crop, d) tuber crops, e) cereals. The changes in the figure are expressed as percentage differences between future (both A2 and B2 scenarios) and present yields.

Table 2
Percentage changes of crop yields for the main Mediterranean regions: N-W = Portugal, Spain, France and Italy, N-E = Serbia, Greece and Turkey, S-E = Jordan, Egypt and Libya, S-W = Tunisia, Algeria and Morocco.

	C4 summer		Legumes		C3 summer		Tubers		Cereals	
	A2-A	B2-A	A2-A	B2-A	A2-A	B2-A	A2-A	B2-A	A2-A	B2-A
N-W	4.2	8.8	−14.4	−4.9	−12.4	−2.8	4.9	7.5	−0.3	4.7
N-E	−0.6	0.2	−7.2	0.9	−5.4	0.9	−9.3	4.4	4.4	12.5
S-E	−7.9	−6.7	−23.3	−30.1	3.7	−0.4	−4.3	−5.7	−4.9	−10.1
S-W	−9.4	−6.4	−23.9	−18.5	−10.3	−4.3	−13.3	−1.5	−3.4	−3.8

crops to escape higher temperature and water stress. The use of longer growing cycle cultivars proved to be a worthy adaptation strategy in future scenarios, where higher temperatures trigger increase of development rate (Fig. 10). Both options, however, would require additional water for irrigation. In particular, the effective use of long cycle cultivars can demand 25–40% more water, which may be not available or not cost effective in the future (Table 3).

4.2. Energy demand

In general, more energy is required for cooling. Over the years the increase in CDD is large in the South Mediterranean (from Gibraltar to Lebanon), i.e., in the Middle East and the North African part of Mediterranean region (Fig. 11). In the northern side, the main increase is in the South Iberian Peninsula, North-Italy–Balkans–Greece, and South Turkey. The seasonal changes in CDDs have also been examined (not shown). As expected the main contribution is from summer, with no increase in winter, and a very small increase in autumn and spring. The only land regions to escape any significant increases in cooling energy demand are south of France, northern part of Turkey (in the proximity of Black Sea), and the northwestern part of Spain. Fig. 12 presents another view on the increase of energy demand by showing the number of days when this demand is needed to cool more than 5 °C. In the southern part of the Mediterranean Sea, from the south of the Iberian Peninsula and North African coast to Syria, an additional month of heavy cooling is required.

In general, less energy is required for heating. Fig. 13 shows the spatial distribution of the general decrease in HDDs. It can be emphasised that:

- The largest decrease occurs in the northern side of the region, from Turkey to North Italy.
- Spain and France see a smaller but still noteworthy decrease.
- The southeast Mediterranean exhibits the lowest decrease, mainly because it is already a warmer region.

Note also the cooling effect of the sea along the coasts. Unlike the CDD rise, the HDD decrease is spread throughout the year (not shown), although this probably depends to some extent on the choice of base temperature. Naturally, winter is the season that will require much less heating. The largest changes occur along and above the axis of North Italy–Balkans–Greece–Turkey. As shown in Fig. 14, the decrease in the number of days that require energy to warm more than 5 °C (HDD>5) varies from about 2 weeks along the coast to a month inland.

4.3. Forest fire risk

The monthly changes of average FWI from May till October between the future and the control period have been examined (not shown). We note that:

- The increase is higher during the summer, with the maximum increase in August in the North Mediterranean inland.
- Balkans, Maghreb, North Adriatic, central Spain, and Turkey seem to be the most vulnerable regions.
- South of France is as strongly affected as Spain, but only in August and September.
- The southeast Mediterranean (from Lebanon to Libya) sees no particular increase or decrease.
- The results are very similar under B2 scenario (not shown).

Fig. 15 shows the increase in the number of days with fire risk (top) and extreme fire risk (bottom).

According to this figure, the increase in the mean FWI is translated into:

- 2–6 additional weeks of fire risk (i.e. more than a month) over all land areas.
- A significant proportion of this increase in fire risk is actually extreme fire risk (FWI>30).
- South of France, and coastal areas of the rest of Mediterranean Region: significant increase in the number of days with fire risk (1–4 weeks), but not in the number of extreme fire risk.

5. Conclusions and wider implications

The climate change in the Mediterranean at the time of a 2 °C global warming has been examined. The basin will experience an average 2 °C warming at the same time as the average globe. The spatial pattern is characterised by larger warming over land areas and slightly lower warming along coastal areas. This fine scale structure is also found with regional models by Giorgi et al. (2004) and Räisänen et al. (2004), both with greater magnitude since their studies cover the later decades in the century (2070–2100).

Strong seasonal dependence is apparent with an average warming up to 4 °C in summer, above 2 °C in autumn and below 2 °C in spring and winter. Studies of European impacts of a CO_2 concentration doubling (Giorgi et al., 1992, Déqué et al., 1998) give similar values. The feature of maximum summer warming in the centres of the Balkans and the Iberian Peninsula appears to be common in climate change simulations (Déqué et al., 1998; Giorgi et al., 2004). The lower in winter and larger in summer temperature anomaly is also a robust finding documented in IPCC reports (IPCC, 2001b, 2007). It is common to both GCMs and RCMs as shown for example by Gibelin and Déqué (2003) for the B2 scenario in 2070–2100 (Hanson et al., 2007; Christensen and Christensen, 2007; Déqué et al., 2007).

The analysis of annual indices of temperature extremes divided the study region in three sub-regions. The northern basin has an additional month of summer and half-month of additional tropical nights. The southern basin has an additional month of both summer and tropical nights. The number of heatwave days (frost nights) increases (decreases) by up to a month inland, but by only 2 weeks along the coast.

Simulated precipitation regimes depict a globally drier Mediterranean in 2030–2060, with a 10–20% drop in annual rainfall. The drop results from a large summer decrease partially balanced by a winter increase in the northern part of the region. The precipitation changes in the intermediate seasons are less pronounced than in winter and summer. In the southern part, the seasonal dependence is smaller. Following the winter precipitation increase in the northern basin, the annual maximum running total rainfall over 3 days shows intensification. Increase in precipitation intensity has been reported in other regions, even in regions where the mean precipitation decreases (Giorgi et al., 2004). The widespread summer negative trend is a common feature of regional climate change simulations (e.g. Jones et al., 1997; Giorgi et al., 2004; Räisänen et al., 2004). However, precipitation changes present large uncertainties, and differences with other simulations are expected.

Nevertheless, our conclusion of a drier Mediterranean in 2031–2060 translates into about 1 week of additional dry days along the coast and in the already dry southeast basin. Over land areas in the northern part, up to and over 3 weeks of additional dry days

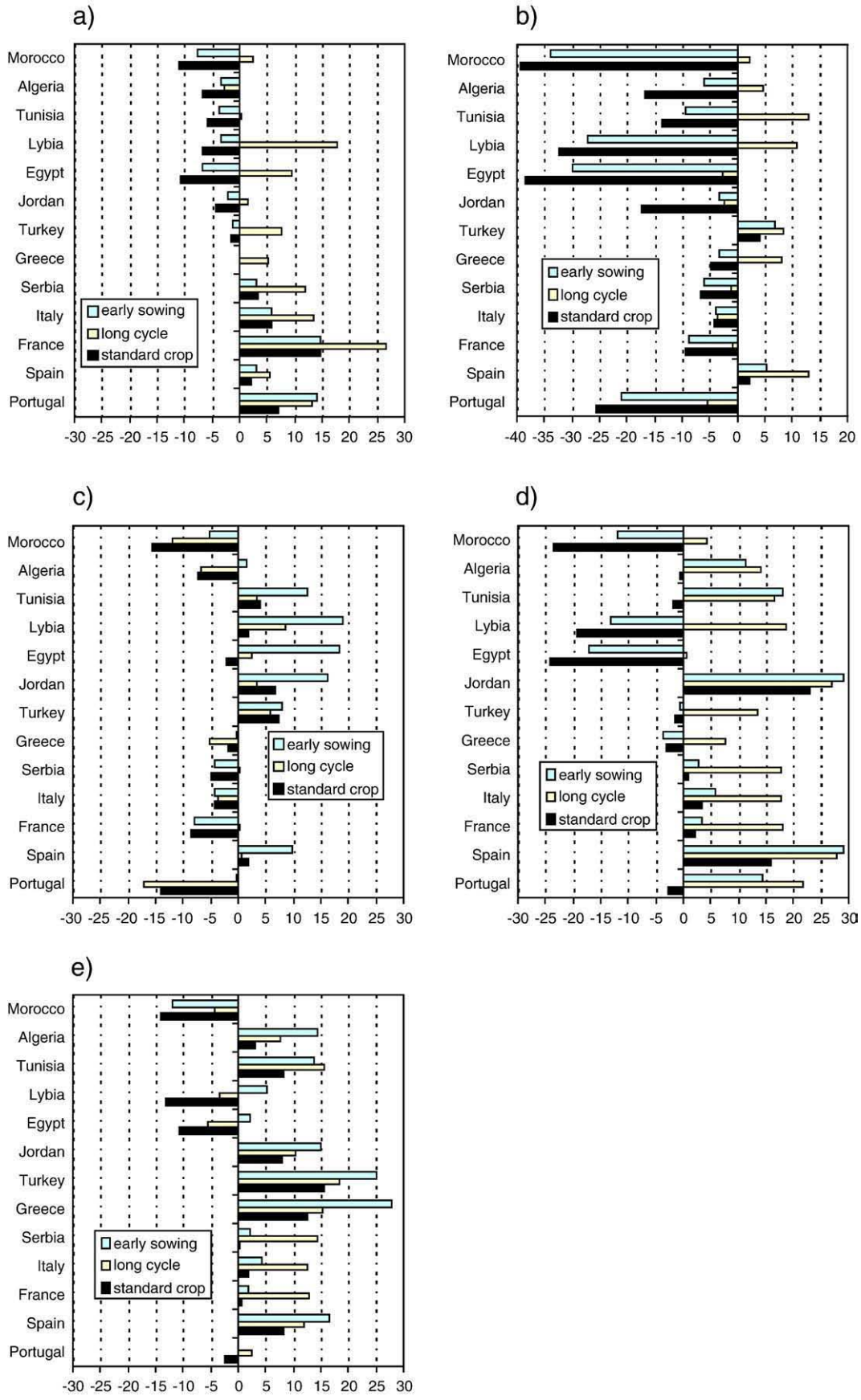

Fig. 10. Impact of different crop adaptation options on crop responses under climate change for: a) C4 summer crop, b) legumes, c) C3 summer crop, d) tuber crops, e) cereals. The changes reported in the figures were expressed as % and obtained as differences between the mean yields of the two futures and the present yields.

Table 3
Mean percentage changes of water supply for irrigated crops under future scenarios for different adaptation options and geographical regions.

Region	Treatment	C4 summer		Tubers	
		A2A-A	B2A-A	A2A-A	B2A-A
N-E	BAU	1.0	−2.7	−9.7	−3.0
	Shorter cycle	−23.8	−30.2	−60.9	−46.4
	Longer cycle	20.1	19.4	46.5	30.8
	Early sowing	0.8	−3.7	−11.0	−3.5
	Late sowing	2.7	0.0	38.0	−2.2
N-W	BAU	14.4	12.7	29.9	13.7
	Shorter cycle	−12.9	−16.1	−23.9	−33.5
	Longer cycle	38.7	38.5	72.7	61.2
	Early sowing	14.4	12.2	29.5	14.4
	Late sowing	15.2	13.2	42.3	16.4
S-E	BAU	−6.3	−4.7	4.5	12.8
	Shorter cycle	−31.3	−30.3	−14.8	−11.7
	Longer cycle	17.6	19.4	28.7	34.7
	Early sowing	−6.8	−6.5	6.5	6.9
	Late sowing	−2.2	0.6	8.1	17.3
S-W	BAU	−1.5	1.8	−4.6	5.7
	Shorter cycle	−23.2	−20.5	−25.0	−17.5
	Longer cycle	19.4	24.5	17.2	30.6
	Early sowing	2.3	5.0	6.9	13.5
	Late sowing	2.8	3.4	−9.3	4.9

Legend: N-W = Portugal, Spain, France and Italy, N-E = Serbia, Greece and Turkey, S-E = Jordan, Egypt and Libya, S-W = Tunisia, Algeria and Morocco.

are projected. No supplementary wet or very wet days are expected. The dry season tends to shift toward autumn, with the exception of the south of France and Algeria where it starts and ends 2 weeks earlier on average. The shift and lengthening of the dry season call for more accurate seasonal analysis through a study on their monthly variations.

Our study has showed that the increases in temperature and reduction in precipitation projected for both future climate scenarios (A2 and B2) leads to a substantial reduction of yields for all the crop types in all the 'hot spots' grid cells, through the reduction of the length of the growing period and the water available for crop growth. For rainfed crops, reductions in yields are more severe in the warmer southern Mediterranean than in the cooler northern Mediterranean, even when the fertilizing effect of increased CO2 was taken into account. However, a different fitting capacity to climate change depending on the specific growth cycle may be highlighted. The higher impacts are generally observed for those crops growing during the summer period (i.e. legumes and C3 summer crops) where the temperature anomaly is up to 4 °C and drought periods are longer. By contrast, winter–autumn crops (cereals) partially escaping the summer higher temperatures and drought, present a prevalent increase in yields.

A warmer climate and its associated increase in CO2 result in small positive impacts on yields of irrigated crops (i.e. C4 and tuber crops) in the northern Mediterranean. However, this trend is followed by an increased water demand, especially for tubers crop in North West area (Table 3). Strategies such as early sowing dates or cultivar with slower development rates may be considered as advisable options to reduce some of the reductions in crop yield determined by the changes in climate conditions. However, for irrigated crops, such options could require up to 40% more water for irrigation, which may or may not be available in the future (Table 3). Moreover, according to recent studies on the effects of tropospheric pollutants such as ozone on crop yields, there is reason to believe that our estimates of yield losses under a future scenario may be conservative. Current and increased concentrations of ground level ozone have been shown to lead to decreases in plant biomass and yield (Gitay et al., 2001; Morgan et al., 2003).

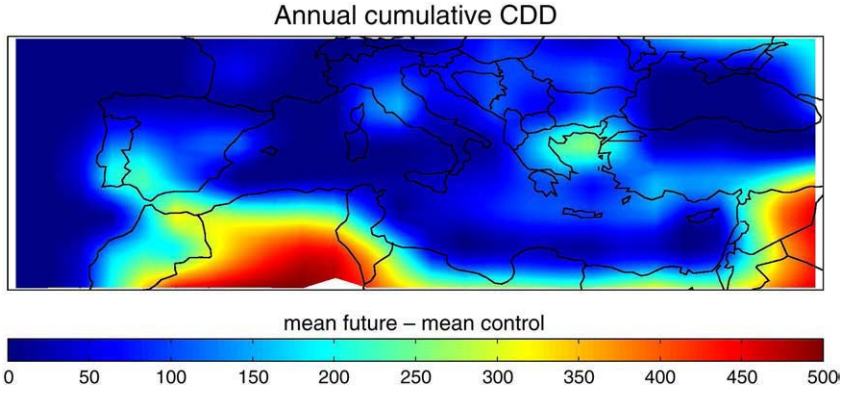

Fig. 11. Changes in average yearly cumulative CDD between the future and control period.

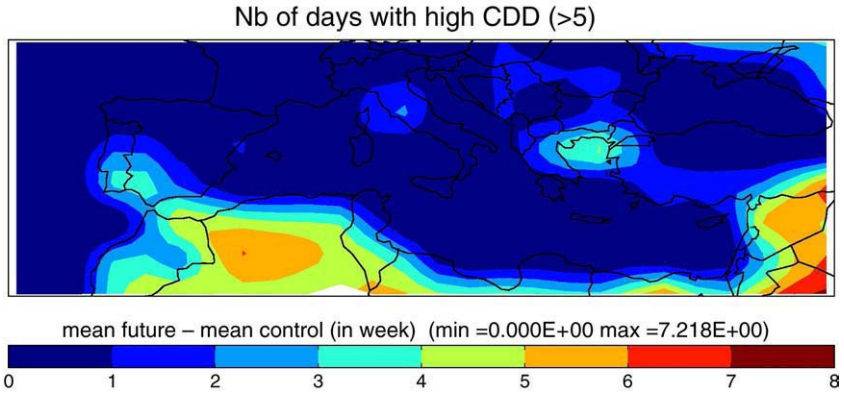

Fig. 12. Changes in the number of days with large cooling demand (CDD>5) between the future and control period.

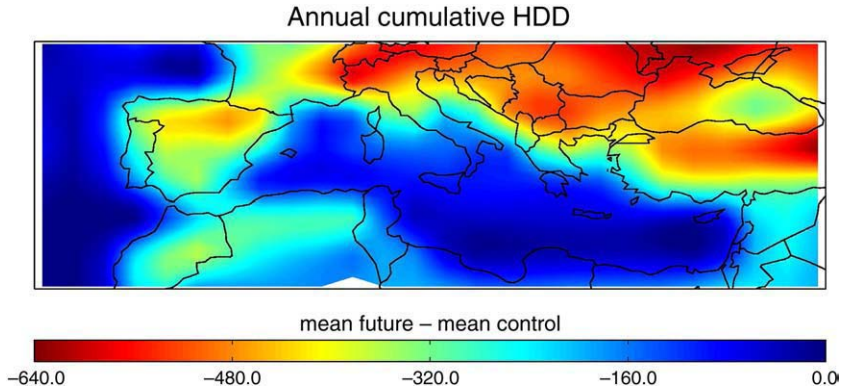

Fig. 13. Changes in average yearly cumulative HDDs between the future and control period.

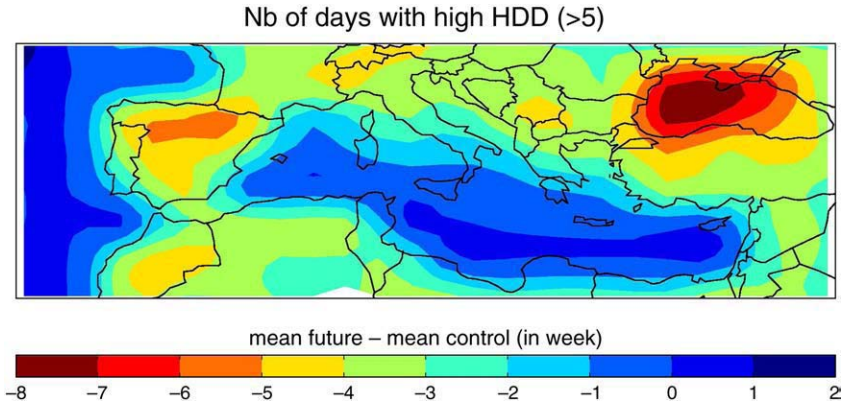

Fig. 14. Changes in the number of days with large heating demand (HDD>5) between the future and control period.

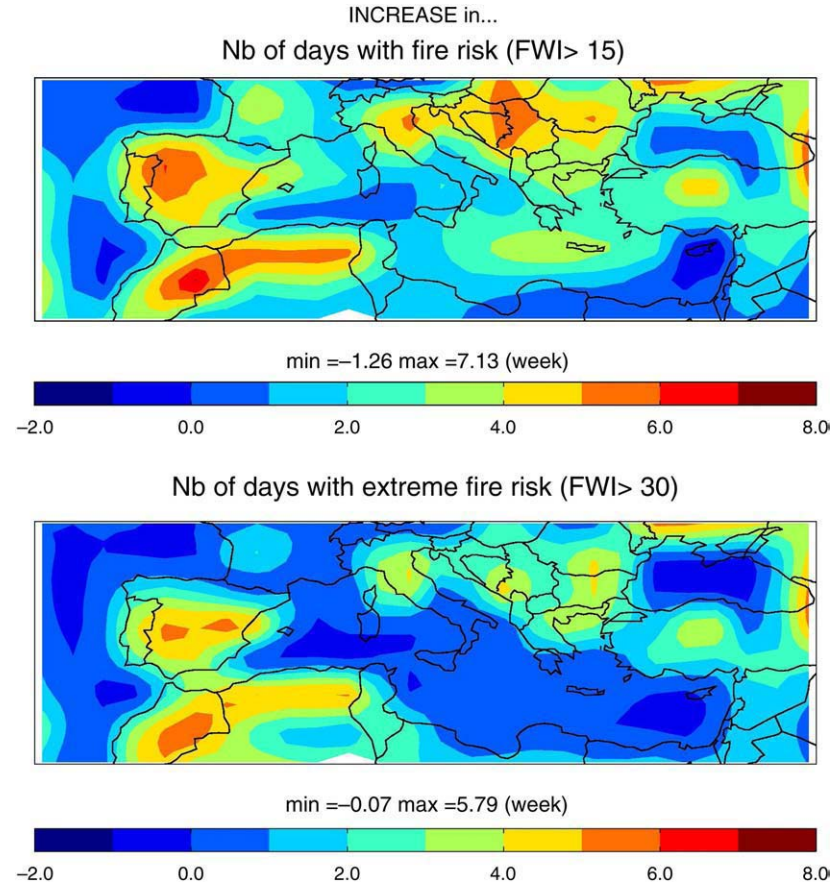

Fig. 15. Changes in the number of weeks with fire risk (top) and extreme fire risk (bottom) between the future and the control period.

Independently of climate change, but exacerbated by it, surface ozone concentrations are expected to increase globally. Thus, if the effects of ozone are to be included in an assessment of crop yields in the Mediterranean under a future climate scenario, the results are likely to be greater yield reductions than presented here.

As expected, the northern Mediterranean region is likely to reduce energy use in the winter due to reduced heating demands. However, during summer, substantial increases in energy demand are expected everywhere, especially in the south. The peak in energy demand hence falls in the dry season, which is expected to become even drier in the future. A low water supply reduces energy production from hydroelectric plants, as well as from conventional power plants, which require water for cooling and for driving the turbines. As a result, energy demands may not be able to be met in the warm period of the year. Additional capacity may need to be installed unless adaptation or mitigation strategies are to put into place. On the other hand, conditions for renewable energy production, such as solar and wind energy, may improve under climate change. The energy demand for cooling is likely to continue to rise as a society becomes richer and increased incomes allow the population to afford more comfort. More air conditioning facilities could be installed. In turn, the heat generated by air conditioning units could raise temperatures further and further increase the demand for cooling.

Rising temperatures over the Mediterranean region in 2031–2060 may well affect the tourism industry, which is of great economic importance for the region. More specifically, the thermal comfort of tourists and their ability to acclimatise to a region prone to high temperatures and heatwaves may be heavily affected. As a result, a gradual decrease in summer tourism in the Mediterranean but an increase in spring and autumn may be expected (Alcamo et al., 2007).

To get a truly additional insight into climatic changes and associated impacts, regional models that account for the topography at regional scales, and particularly coastline features, are required. This is of great importance especially for precipitation patterns that already show high regional variability in the contemporaneous climate and particularly in areas with contrasted topography near coastland (Türkeş, 1998; Romero et al., 1999; Xoplaki et al., 2000; Kostopoulou and Jones, 2005). Finally, weighted multi-model ensembles of simulations would provide a more robust assessment of climatic changes. The ENSEMBLES EU-project allows this type of study to be repeated using multiple Regional Climate Models (www.ensembles-eu.org), thus producing a more thorough and robust assessment of climate changes and impacts in the Mediterranean basin.

Acknowledgments

This work was supported by WWF International and by the European Commission ENSEMBLES project (Contract number GOCE-CT-2003-505539, www.ensembles-eu.org).

References

Ainsworth, E.A., Long, S.P., 2005. What have we learned from 15 years of free-air CO_2 enrichment (FACE)? A meta-analytic review of responses to rising CO_2 in photosynthesis, canopy properties and plant production. New Phytologist 165, 351–372.

Alcamo, J., Moreno, J.M., Nováky, B., Bindi, M., Corobov, R., Devoy, R.J.N., Giannakopoulos, C., Martin, E., Olesen, J.E., Shvidenko, A., 2007. Europe. Climate change 2007: impacts, adaptation and vulnerability. In: Parry, M.L., Canziani, O.F., Palutikof, J.P., van der Linden, P.J., Hanson, C.E. (Eds.), Contribution of Working Group II to the Fourth Assessment Report of the Intergovernmental Panel on Climate Change (IPCC). Cambridge University Press, Cambridge, UK, pp. 541–580.

Beniston, M., 2004. The 2003 heatwave in Europe: a shape of things to come? An analysis based on Swiss climatological data and model simulations. Geophysical Research Letters 31 (L02202). doi:10.1029/2003GL018857.

Bolle, H.-J., 2003. Mediterranean climate. Variability and Trends. Springer, Berlin.

Christensen, J.H., Christensen, O.B., 2007. A summary of the PRUDENCE model projections of changes in European climate by the end of this century. Climatic Change 81, 7–30.

Christensen, J.H., Carter, T.R., Giorgi, F., 2002. PRUDENCE employs new methods to assess European climate change. EOS 83, 147.

Déqué, M., Marquet, P., Jones, R.G., 1998. Simulation of climate change over Europe using a global variable resolution general circulation model. Climate Dynamics 14, 173–189.

Deque, M., Jones, R.G., Wild, M., Giorgi, F., Christensen, J.H., Hassell, D.C., Vidale, P.L., Rockel, B., Jacob, D., Kjellstrom, E., de Castro, M., Kucharski, F., van den Hurk, B., 2005. Global high resolution versus limited area model climate change scenarios over Europe: quantifying confidence level from PRUDENCE results. Climate Dynamics 25, 653–670.

Déqué, M., Rowell, D.P., Lüthi, D., Giorgi, F., Christensen, J.H., Rockel, B., Jacob, D., Kjellström, E., de Castro, M., van den Hurk, B., 2007. An intercomparison of regional climate simulations for Europe: assessing uncertainties in model projections. Climatic Change 81, 53–70.

Diffenbaugh, N.S., Pal, J.S., Giorgi, F., Gao, X., 2007. Heat stress intensification in the Mediterranean climate change Hotspot. Geophysical Research Letters 34 (L11706). doi:10.1029/2007GL030000.

Fontaine, B., Philippon, N., Camberlin, P., 1999. An improvement of June–September rainfall forecasting in the Sahel based upon region April–May moist static energy content (1968–1997). Geophysical Research Letters 26, 2041–2044.

Founda, D., Papadopoulos, K.H., Petrakis, M., Giannakopoulos, C., Good, P., 2004. Analysis of mean, maximum and minimum temperatures in Athens from 1897 to 2001 with emphasis to the last decade: trends, warm and cold events. Global and Planetary Change 44, 27–38.

Friedlingstein, P., Dufresne, J.-L., Cox, P.M., Rayner, P., 2003. How positive is the feedback between climate change and the carbon cycle? Tellus 55B, 692–700.

Gao, X., Giorgi, F., 2008. Increased aridity in the Mediterranean region under greenhouse gas forcing estimated from high resolution regional climate projections. Global and Planetary Change 62, 195–209.

Gao, X., Pal, J.S., Giorgi, F., 2006. Projected changes in mean and extreme precipitation over the Mediterranean region from high resolution double nested RCM simulations. Geophysical Research Letters 33 (L03706). doi:10.1029/2005GL024954.

Giannakopoulos, C., Psiloglou, B., 2006. Trends in energy load demand for Athens, Greece: weather and non-weather related factors. Climate Research 13, 97–108.

Gibelin, A.-L., Déqué, M., 2003. Anthropogenic climate change over the Mediterranean region simulated by a global variable resolution model. Climate Dynamics 20, 327–339.

Giorgi, F., 2006. Climate change Hot-Spots. Geophysical Research Letters 33 (L08707). doi:10.1029/2006GL025734.

Giorgi, F., Bi, X., 2005. Updated regional precipitation and temperature changes for the 21st century from ensembles of recent AOGCM simulations. Geophysical Research Letters 32 (L21715). doi:10.1029/2005GL024288.

Giorgi, F., Marinucci, M.R., Visconti, G., 1992. A $2XCO_2$ climate change scenario over Europe generated using a limited area model nested in a general circulation model 2. Climate change scenario. Journal of Geophysical Research 97, 10011–10028. doi:10.1029/92JD00614.

Giorgi, F., Bi, X.Q., Pal, J., 2004. Mean, interannual variability and trends in a regional climate change experiment over Europe. II: climate change scenarios (2071–2100). Climate Dynamics 23, 839–858.

Gitay, H., Brown, S., Easterling, W., Jallow, B., 2001. Ecosystems and their goods and services. In: McCarthy, J.J., Canziani, O.F., Leary, N.A., Dokken, D.J., White, K.S. (Eds.), Climate Change 2001: Impacts, Adaptation and Vulnerability, pp. 735–800.

Good, P., Moriondo, M., Giannakopoulos, C., Bindi, M., 2008. The meteorological conditions associated with extreme fire risk in Italy and Greece: relevance to climate model studies. International Journal of Wildland Fire 17, 155–165.

Gordon, C., Cooper, C., Senior, C.A., Banks, H., Gregory, J.M., Johns, T.C., Mitchell, J.F.B., Wood, R.A., 2000. The simulation of SST, sea ice extents and ocean heat transports in a version of the Hadley Centre coupled model without flux adjustments. Climate Dynamics 16, 147–168.

Hanson, C.E., Palutikof, J.P., Livermore, M.T.J., Barring, L., Bindi, M., Corte-Real, J., Duaro, R., Giannakopoulos, C., Holt, T., Kundzewicz, Z., Leckebusch, G., Radziejewski, M., Santos, J., Schlyter, P., Schwarb, M., Stjernquist, I., Ulbrich, U., 2007. Modeling the impact of climate extremes: an overview of the MICE project. Climatic Change 81, 163–177 PRUDENCE Special Issue.

IPCC, 2001a. Climate change 2001: impacts, adaptation and vulnerability. In: McCarthy, J.J., Canziani, O.F., Leary, N.A., Dokken, D.J., White, K.S. (Eds.), Contribution of Working Group II to the Third Assessment Report of the Intergovernmental Panel on Climate Change. Cambridge University Press, Cambridge. 1032 pp.

IPCC, 2001b. Climate change 2001: the scientific basis. In: Houghton, J.T., Ding, Y., Griggs, D.J., Noguer, M., Van der Linden, P.J., Dai, X., Maskell, K., Johnson, C.A. (Eds.), Contribution of Working Group I to the Third Assessment Report of the Intergovernmental Panel on Climate Change. Cambridge University Press, Cambridge. 881 pp.

IPCC, 2007. Climate change 2007: the physical science basis. In: Solomon, S., Qin, D., Manning, M., Chen, Z., Marquis, M., Averyt, K.B., Tignor, M., Miller, H.L. (Eds.), Contribution of Working Group I to the Fourth Assessment Report of the Intergovernmental Panel on Climate Change. Cambridge University Press, Cambridge. 996 pp.

Jones, R.G., Murphy, J.M., Noguer, M., Keen, A.B., 1997. Simulation of climate change over Europe using a nested regional-climate model. II: comparison of driving and regional model responses to a doubling of carbon dioxide. Quarterly Journal of the Royal Meteorological Society 123, 265–292.

Jones, C.D., Cox, P.M., Essery, R.L.H., Roberts, D.L., Woodage, M.J., 2003a. Strong carbon cycle feedbacks in a climate model with interactive CO2 and sulphate aerosols. Geophysical Research Letters 30. doi:10.1029/2003GL016867.

Jones, C.D., Cox, P.M., Huntingford, C., 2003b. Uncertainty in climate–carbon cycle projections associated with the sensitivity of soil respiration to temperature. Tellus 55B, 642–648.

Kadioğlu, M., Şen, Z., Gültekin, L., 2001. Variations and trends in Turkish seasonal heating and cooling degree-days. Climatic Change 49, 209–223.

Kimball, B.A., Kobayashi, K., Bindi, M., 2002. Responses of agricultural crops to free-air CO_2 enrichment. Advances in Agronomy 77, 293–368.

Kostopoulou, E., Jones, P.D., 2005. Assessment of climate extremes in the eastern Mediterranean. Meteorology and Atmospheric Physics 89, 69–85.

Lionello, P., Malanotte, P., Boscolo, R. (Eds.), 2006. Mediterranean Climate Variability. Elsevier B.V., Amsterdam.

Morgan, P.B., Ainsworth, E.A., Long, S.P., 2003. How does elevated ozone impact soybean? A meta-analysis of photosynthesis, growth and yield. Plant Cell and Environment 26, 1317–1328.

Moriondo, M., Good, P., Durao, R., Bindi, M., Giannakopoulos, C., Corte-Real, J., 2006. Potential impact of climate change on fire risk in the Mediterranean area. Climate Research 31, 85–95.

Mudelsee, M., Alkio, M., 2007. Quantifying effects in two-sample environmental experiments using bootstrap confidence intervals. Environmental Modelling & Software 22, 84–96.

Nakicenovic, N., Alcamo, J., Davis, G., de Vries, B., Fenhann, J., Gaffin, S., Gregory, K., Grübler, A., Jung, T.Y., Kram, T., La Rovere, E.L., Michaelis, L., Mori, S., Morita, T., Pepper, W., Pitcher, H., Price, L., Raihi, K., Roehrl, A., Rogner, H.H., Sankovski, A., Schlesinger, M., Shukla, P., Smith, S., Swart, R., van Rooijen, S., Victor, N., Dadid, Z., 2000. Emissions Scenarios. A Special Report of Working Group III of the Intergovernmental Panel on Climate Change. Cambridge University Press, Cambridge, U.K. 599 pp. Available online at: http://www.grida.no/climate/ipcc/emission/index.htm.

New, M., 2005. Arctic climate change with a 2 °C global warming. In: Rosentrater, L.D., New, M., Kaplan, J.O., Comiso, J.C., Watt-Cloutier, S., et al. (Eds.), Evidence and Implications of Dangerous Climate Change in the Arctic. WWF International Arctic Program, Oslo, pp. 1–15.

Pinol, J., Terradas, J., Lloret, F., 1998. Climate warming, wildfire hazard, and wildfire occurrence in coastal eastern Spain. Climatic Change 38, 345–357.

Pope, V.D., Gallani, M.L., Rowntree, P.R., Stratton, R.A., 2000. The impact of new physical parameterizations in the Hadley Centre climate model: HadAM3. Climate Dynamics 16, 123–146.

Räisänen, J., Hansson, U., Ullerstig, A., Döscher, R., Graham, L.P., Jones, C., Meier, M., Samuelsson, P., Willén, U., 2003. GCM driven simulations of recent and future climate with the Rossby Centre coupled atmosphere Baltic Sea regional climate model RCAO. SMHI Reports Meteorology and Climatology 101, SMHI, SE 60176 Norrköping, Sweden. 61 pp.

Räisänen, J., Hansson, U., Ullerstig, A., Döscher, R., Graham, L.P., Jones, C., Meier, H.E.M., Samuelsson, P., Willén, U., 2004. European climate in the late 21st century: regional simulations with two driving global models and two forcing scenarios. Climate Dynamics 22, 13–31.

Romero, R., Ramis, C., Guijarro, J.A., 1999. Daily rainfall patterns in the Spanish Mediterranean area: an objective classification. International Journal of Climatology 19, 95–112.

Schär, C., Vidale, P., Lüthi, D., Frei, C., Häberli, C., Liniger, M.A., Appenzeller, C., 2004. The role of increasing temperature variability for European summer heatwaves. Nature 427, 332–336.

Smith, J.B., Schellnhuber, H.-J., et al., 2001. Vulnerability to climate change and reasons for concern: a synthesis. In: McCarthy, J.J., Canziani, O.F., Leary, N.A., Dokken, D.J., White, K.S. (Eds.), Climate Change 2001: Impacts, Adaptation, and Vulnerability: Contribution of Working Group II to the Third Assessment Report of the Intergovernmental Panel on Climate Change. Cambridge University Press, Cambridge, pp. 913–967.

Stockle, C.O., Donatelli, M., Nelson, R., 2003. CropSyst, a cropping systems simulation model. European Journal of Agronomy 18, 289–307.

Türkeş, M., 1998. Influence of geopotential heights, cyclone frequency and Southern Oscillation on rainfall variations in Turkey. International Journal of Climatology 18, 649–680.

Valor, E., Meneu, V., Caselles, V., 2001. Daily air temperature and electricity load in Spain. Journal of Applied Meteorology 40 (8), 1413–1421.

van Wagner, C.E., 1987. Development and structure of the Canadian forest fire weather index system. Canadian Forestry Service, Forestry Technical Report35.

Viegas, D.X., Bovio, G., Ferreira, A., Nosenzo, A., Sol, B., 1999. Comparative study of various methods of fire danger evaluation in Southern Europe. International Journal of Wildland Fire 9, 235–246.

Viegas, D.X., Pinol, J., Viegas, M.T., Ogaya, R., 2001. Estimating live fine fuels moisture content using meteorologically-based indices. International Journal of Wildland Fire 10, 223–240.

Wilby, R.L., Wigley, T.M.L., Conway, D., Jones, P.D., Hewitson, B.C., Main, J., Wilks, D.S., 1998. Statistical downscaling of general circulation model output: a comparison of methods. Water Resources Research 34, 2995–3008.

Xoplaki, E., Luterbacher, J., Burkard, R., Patrikas, I., Maheras, P., 2000. Connection between the large scale 500 hPa geopotential height fields and precipitation over Greece during wintertime. Climate Research 14, 129–146.